Supporting Information

pH-Responsive Charge-Conversional and Hemolytic Activities of Magnetic Nanocomposite Particles for Cell-Targeted Hyperthermia

Md. Abdur Rahman,[1] Yoshimasa Matsumura,[1] Shigekazu Yano,[2] Bungo Ochiai[1*]

[1]Department of Chemistry and Chemical Engineering, Graduate School of Science and Engineering, Yamagata University, 4-3-16, Jonan, Yonezawa, Yamagata 992-8510, Japan

[2]Department of Biochemical Engineering, Graduate School of Science and Engineering, Yamagata University, 4-3-16, Jonan, Yonezawa, Yamagata 992-8510, Japan

Contents **Pages**

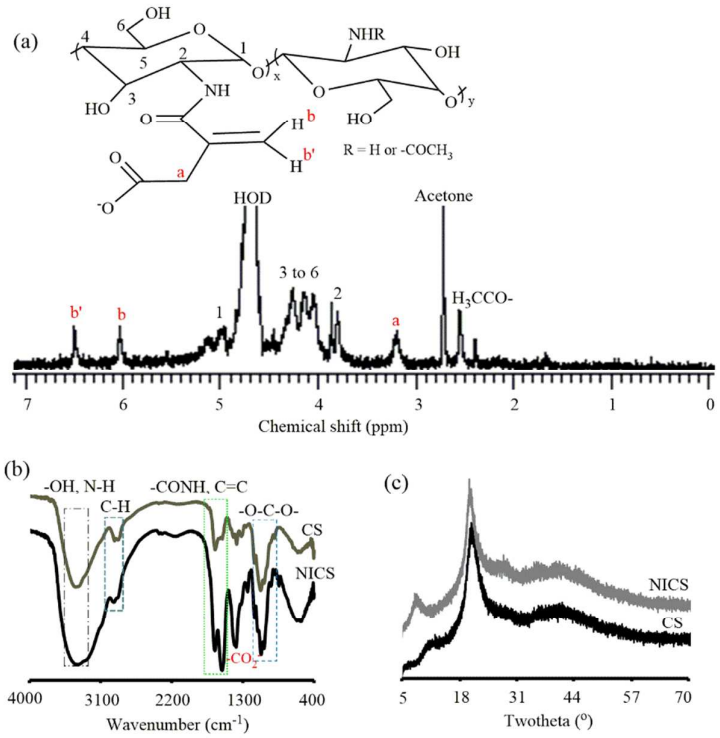

Figure S1. Characterization of NICS by (a) ^{1}H NMR spectrum (D_2O, 90 °C, 400 MHz), (b) FTIR spectra of NICS and CS (KBr disk), and (c) XRD patterns of NICS and CS.

^{1}H NMR (Figure S1$_a$): The itaconization degree of CS was calculated to be 36% by using reported method.[1] The spectrum of CS was not measurable under this condition because of insolubility in water due to the strong intermolecular hydrogen bonding originates from high deacetylation degree.

FTIR (Figure S1$_b$): A characteristic new peak appeared in the FTIR spectrum of NICS at 1382 cm^{-1} assignable to the carbonyl stretching of -CO_2^- ions originating from itaconization of CS via neutralization with NaOH aq. In addition, the O-H, N-H, and -CONH- peaks were significantly changed from the CS spectrum.

XRD (Figure S1$_c$): The XRD spectrum of CS shows a very weak reflection at 11° and a strong reflection at 21°, which are assignable to the crystal forms I and II of CS, respectively.[2] Therefore, CS has semicrystalline structure. However, the XRD pattern of NICS showed a medium intense diffraction band at 8.5°, and a strong reflection centred at 20° and no any significant peak observable at 11°. The absence of a signal at 11° and the change in peak position suggested that the crystal structure of CS was interrupted because of the insertion of hydrophilic *N*-itaconyl moieties. This outcome demonstrated that intermolecular hydrogen bonding was significantly lowered in NICS than that in CS resulting better dispersibility in water.

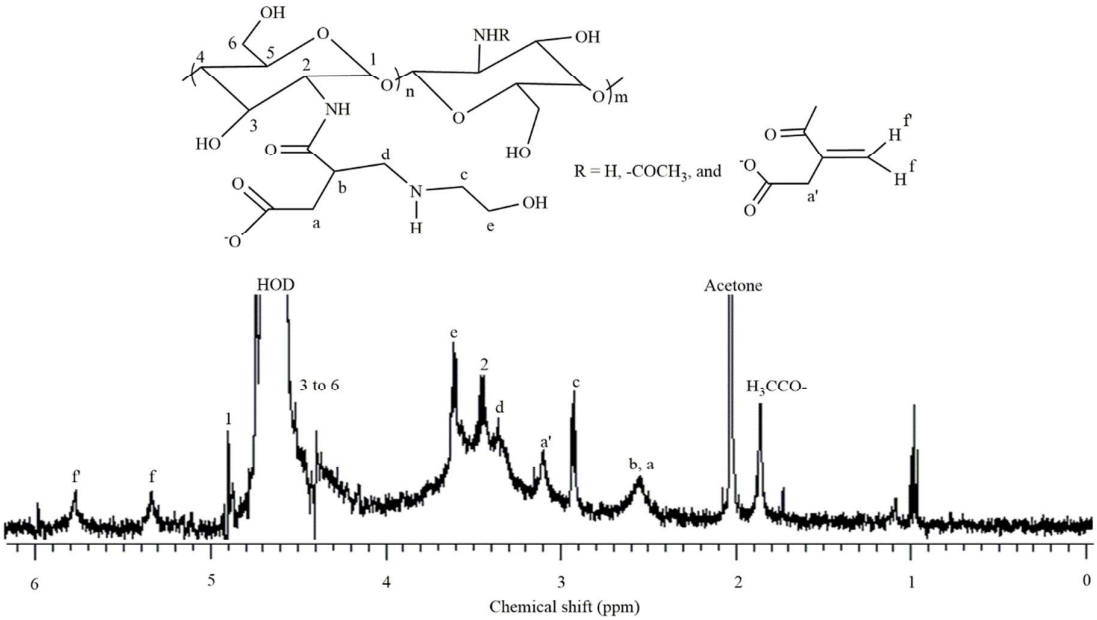

Figure S2. ^{1}H NMR spectrum of NICS-EA (D_2O, 25 °C, 400 MHz).

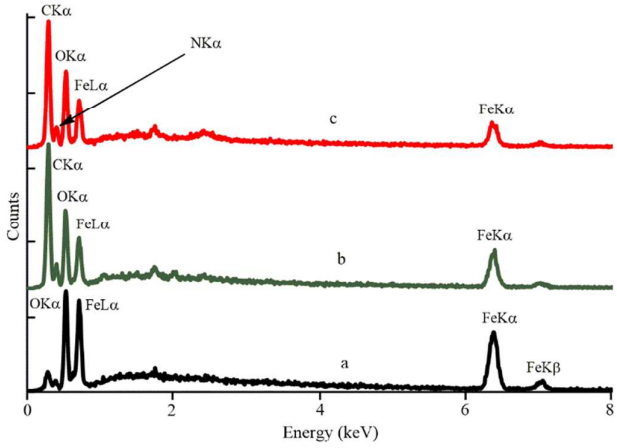

Figure S3. EDX spectra of (a) bare Fe_3O_4, (b) Fe_3O_4-NICS-EGDE, and (c) charge-conversional Fe_3O_4-NICS-EGDE-EA nanocomposite particles.

Samples were placed on a carbon tape for EDX analysis. As a result, the intensities of C and O signals are not quantitative. The peaks of C, O, Fe, and N are clearly visible in the spectra.

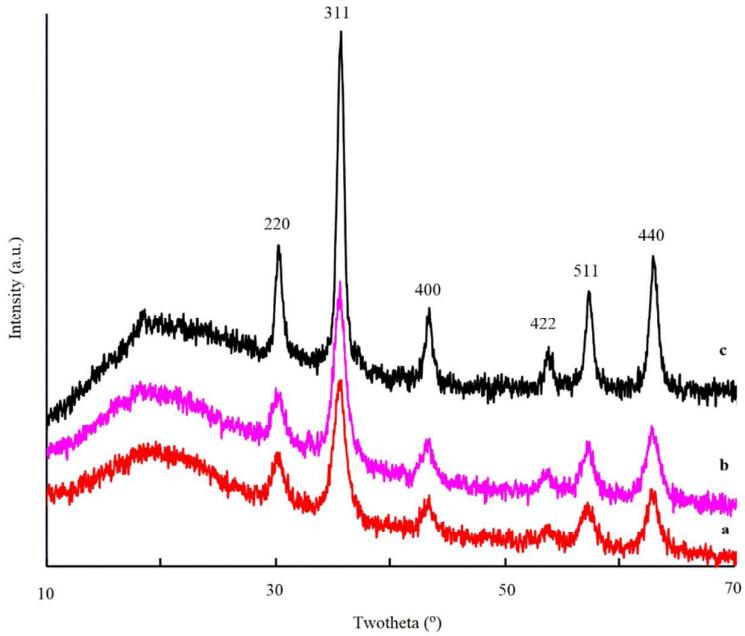

Figure S4. XRD analysis of (a) bare Fe_3O_4, (b) Fe_3O_4-NICS-EGDE, and (c) charge-conversional Fe_3O_4-NICS-EGDE-EA nanocomposite particles.

All of the XRD pattern shows six characteristice reflections assignable to the (220), (311), (400), (422), (511), and (440) lattice planes of spinel Fe_3O_4 (JCPDS no. 88-0315)[3] and any significant peaks originating from other iron compounds were not observable.[4]

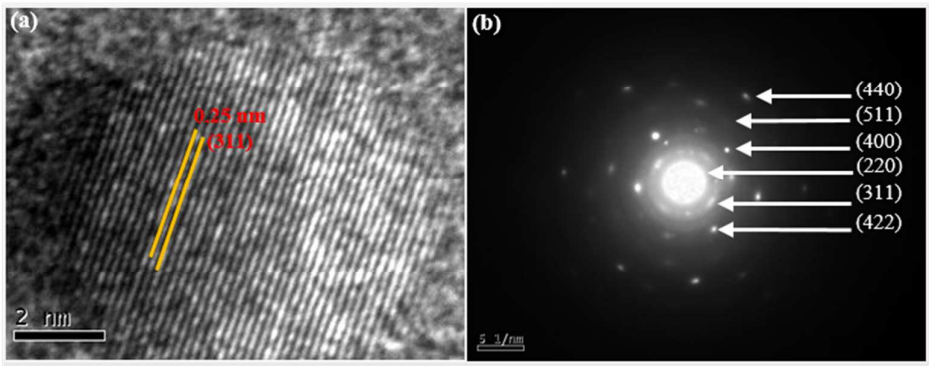

Figure S5. Unit cell characterization of charge-conversional Fe_3O_4-NICS-EGDE-EA nanocomposite particles by (a) HRTEM micrograph, and (b) SAED patterns.

The HRTEM micrograph (Figure $S5_a$) of a single charge-conversional Fe_3O_4-NICS-EGDE-EA nanocomposite particle indicating the vivid lattice fringes with interplanar spacing of 0.25 nm assignable to the (311) plane. A typical SAED pattern shows clear spots, assignable to the six Miller indices (*hkl*) calculated from d-spacing revealed the monocrystalline nature of the core Fe_3O_4 that agrees with the XRD data (Figure $S5_b$).

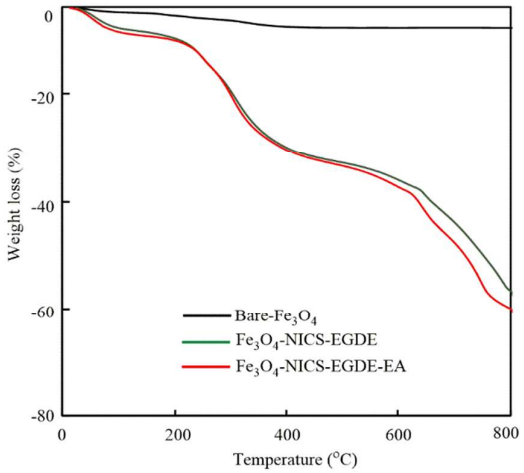

Figure S6. TGA profiles of (a) bare Fe_3O_4, (b) Fe_3O_4-NICS-EGDE, and (c) charge-conversional Fe_3O_4-NICS-EGDE-EA nanocomposite particles (10 °C min^{-1}, N_2).

The amounts of polymer-coating materials present in Fe_3O_4-NICS-EGDE and charge-conversional Fe_3O_4-NICS-EGDE-EA nanocomposite particles were estimated using TGA (Figure S6). Synthesized bare Fe_3O_4 is highly thermo-stable, and the total weight loss was 4% below 450 °C, because of the desorption of physically and chemically bound water. Significant weight loss was invisible in the range of 450 to 800 °C. The TGA profiles of both composites revealed a significant three-stage weight loss with respect to their initial weights. The first 7% weight loss below 200 °C, is assignable to the removal of adsorbed water. The second-stage weight loss of 34 and 35% in the range of 200 to 600 °C are corresponded to the degradation of the coating materials. The final 55% and 59% weight loss are attributed to the coating-materials-induced catalytic degradation of core Fe_3O_4 to γ- Fe_2O_3 and FeO.[5]

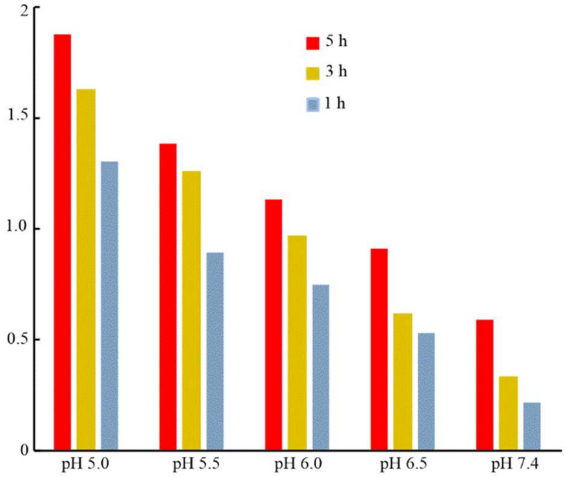

Figure S7. Time-dependent hemolysis of sheep RBCs by charge-conversional Fe_3O_4-NICS-EGDE-EA nanocomposite particles (600 μg ml^{-1}, 0.150 M $NaCl_{(aq)}$, 37 °C).

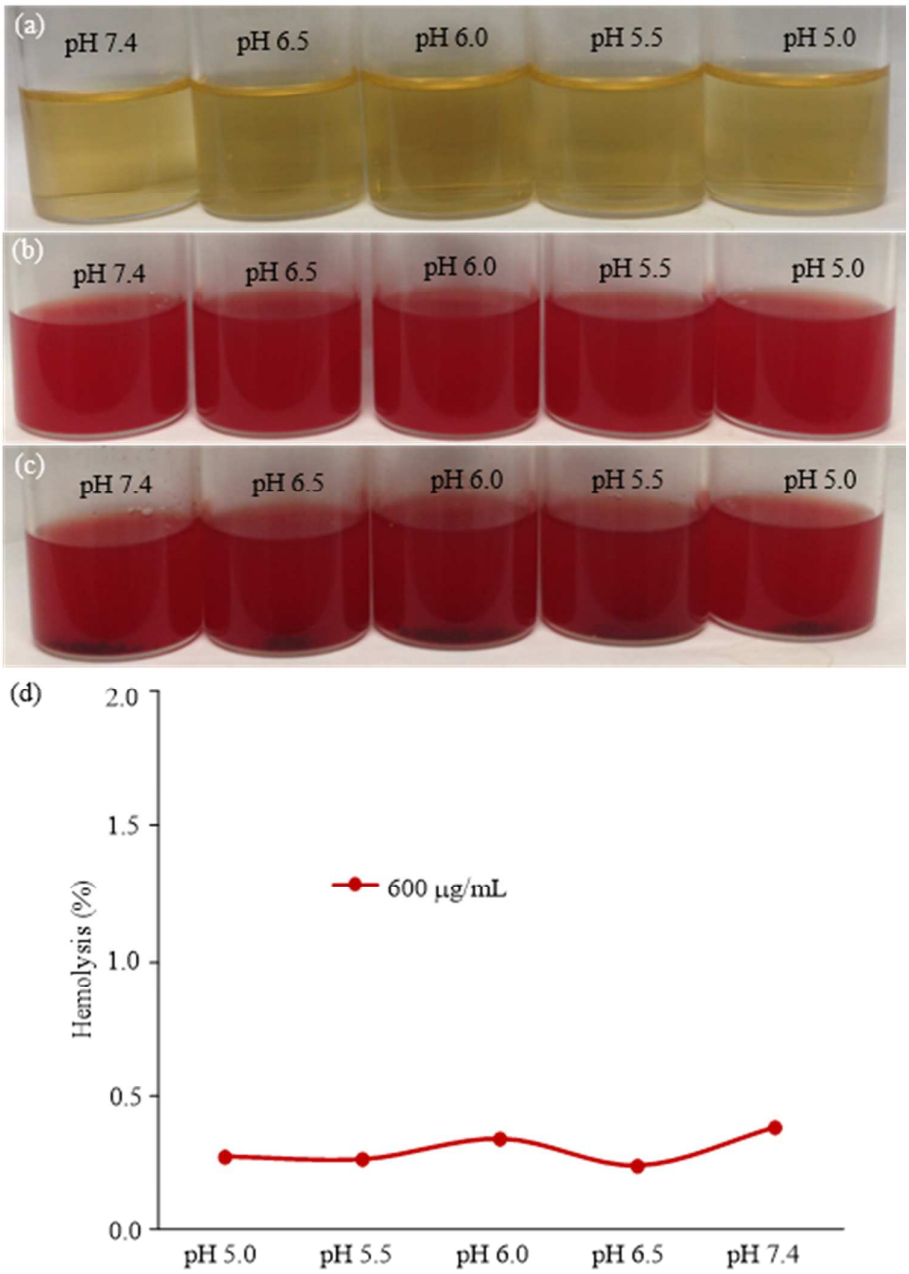

Figure S8. Photo images of the dispersity of Fe_3O_4-NICS-EGDE (a) dispersed in saline, (b) just after addition of RBCs, and (c) incubated at 37 °C for 5 h resulting into aggregation, and pH-dependent (d) hemolytic activities of unmodified Fe_3O_4-NICS-EGDE nanocomposite particles.

The aggregates of the unmodified Fe_3O_4-NICS-EGDE nanocomposite particles were observed as black precipitates (Figure S8c). The unmodified Fe_3O_4-NICS-EGDE nanocomposite particles showed low hemolytic activities (below 0.5%) because of their aggregation in the RBC dispersion resulted in negligible interaction with dispersed RBCs.

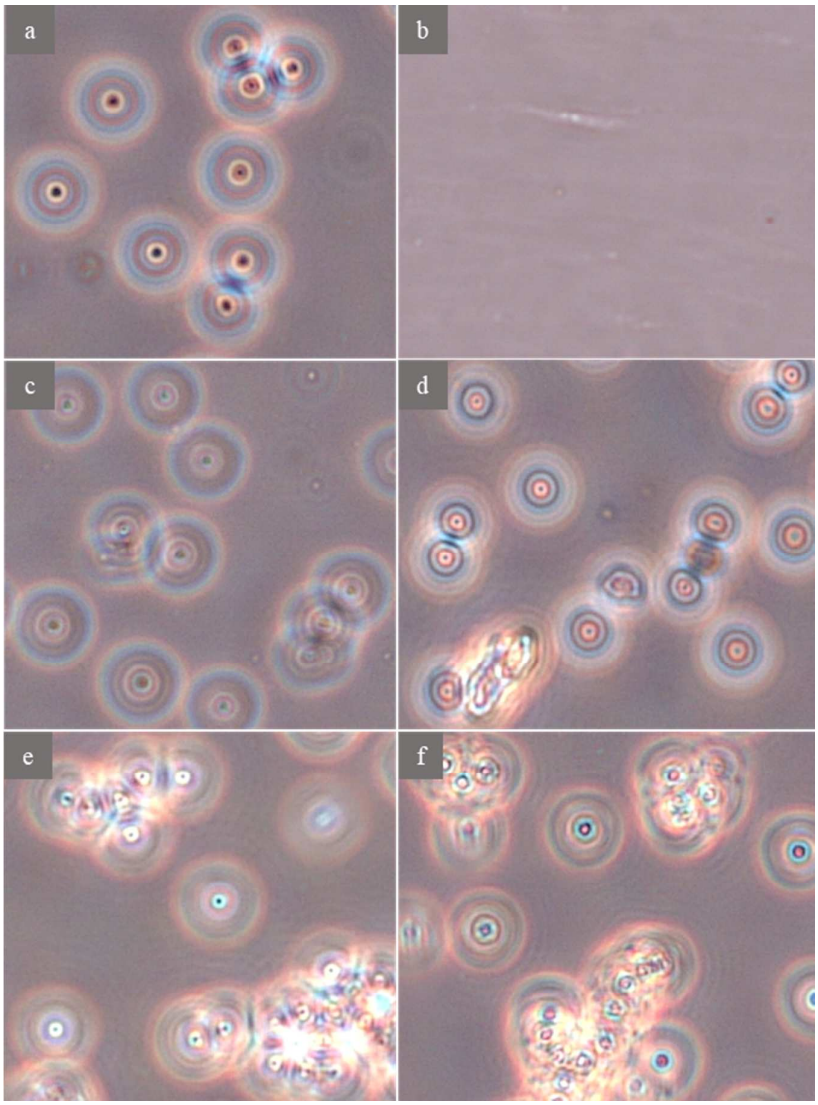

Figure S9. Light microscopic images of hemolysis of the sheep RBCs by charge-conversional Fe_3O_4-NICS-EGDE-EA nanocomposite particles: (a) negative control, (b) positive control (1% triton $X100_{aq.}$), incubated at pH 5.0 for (c) 0 h, (d) 1 h, (e) 3 h, and (f) 5 h with 600 µg mL^{-1} nanocomposite.

Just after treatment with the dispersion of charge-conversional Fe_3O_4-NICS-EGDE-EA nanocomposite particles (0 h), RBCs showed their normal biconcave disk shape almost similar to the control cells (Figure $S9_{a,c}$). A gradual membrane disruption was proceeded (Figure $S9_{d-f}$) with the progression of time (1, 3, and 5 h) at the highest concentration (600 µg mL^{-1}) under study. These observations support the pH-dependent hemolysis data and suggested that the charge-conversional Fe_3O_4-NICS-EGDE-EA nanocomposite particles have very negligible hemolytic activity at physiological conditions, while they are hemolytic at lower pH.

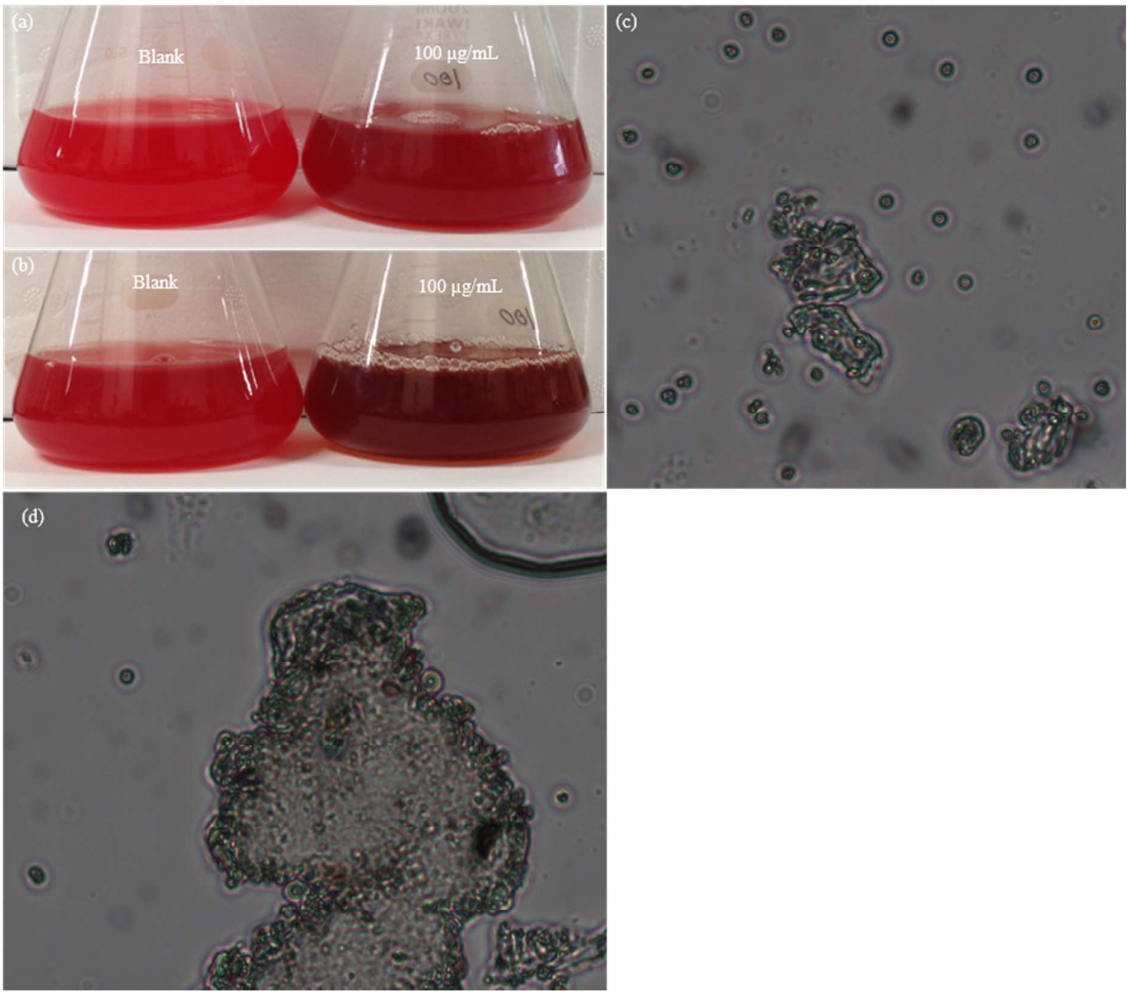

Figure S10. Membranolysis of sheep RBCs by the charge-conversional Fe_3O_4-NICS-EGDE-EA nanocomposite particles (a,b) optical images, and (c,d) light microscopic images after MW irradiation at pH 6.8 (zeta potential = -13 mV), and pH 6.5 (zeta potential = -7 mV), respectively.

References:

1. Sashiwa, H.; Shigemasa, Y. Chemical Modification of Chitin and Chitosan 2: Preparation and Water Soluble Property of *N*-Acylated or *N*-Alkylated Partially Deacetylated Chitins. *Carbohydr. Polym.* 1999, 39, 127-138.
2. Zhu, A.; Chen, T.; Yuan, L.; Wu, H.; Lu, P. Synthesis and Characterization of *N*-Succinyl-Chitosan and its Self-Assembly of Nanospheres. *Carbohydr. Polym*. 2006, 66, 274-279.
3. Wu, J.; Yang, J. Superlong Salicylideneaniline Semiconductor Nanobelts Prepared by a Magnetic Nanoparticle-Assisted Self-Assembly Process for Luminescence Thermochromism. *ACS Omega* 2017, 2, 2264-2272.
4. Dolatkhah, A.; Wilson, L. D. Magnetite/Polymer Brush Nanocomposites with Switchable Uptake Behavior Toward Methylene Blue. *ACS Appl. Mater. Interface* 2016, 8, 5595-5607.
5. Rahman, M. A.; Ochiai, B. Fabrication and Hemocompatibility of Carboxy-Chitosan Stabilized Magnetite Nanoparticles. *Microsyst. Technol.* 2017, DOI:10.1007/s00542-017-3318-8**.**